OKU Fen Bilimleri Enstitüsü Dergisi
7(5): 2053-2064, 2024

OKU Journal of The Institute of Science and Technology, 7(5): 2053-2064, 2024

Osmaniye Korkut Ata Üniversitesi Fen Bilimleri Enstitüsü Dergisi

Osmaniye Korkut Ata University Journal of The Institute of Science and Technology

Examination of the Electrochemical Behavior of Ru Nanoparticles Prepared on MgO

Gamze BOZKURT[1*]

[1]Project Coordination Implementation and Research Center, Erzurum Technical University, Erzurum, Türkiye

[1]https://orcid.org/0000-0003-2128-9934
*Corresponding author: gamze.bozkurt@erzurum.edu.tr

Research Article

Article History:
Received: 07.03.2024
Accepted: 10.05.2024
Published online: 10.12.2024

Keywords:
Ru/MgO
Electrochemical
Microemulsion

ABSTRACT

Electrode materials are an important component for the performance and life of electrochemical devices. Various metal and metal oxide materials are used as electrode materials for electrochemical devices. In this context, various studies are being carried out to improve the electrochemical properties of these materials. In this study, Ru/MgO metal/metal oxide nanomaterial was synthesized for energy storage devices, and electrochemical properties of Ru/MgO nanomaterial was examined by cyclic voltammetry (CV) and galvanostatic charge and discharge (GCD) methods. Homogeneous Ru nanoparticles were obtained on MgO. According to the calculation made using the XRD pattern, the crystal size of Ru nanoparticles was approximately 4.2 nm. According to GCD measurements taken at different current densities, the highest specific capacitance was obtained with 239 F/g at 0.5 A/g.

MgO Üstüne Hazırlanan Ru Nanopartiküllerin Elektrokimyasal Özelliklerinin İncelenmesi

Araştırma Makalesi

Article History:
Received: 07.03.2024
Accepted: 10.05.2024
Published online: 10.12.2024

Anahtar Kelimeler;
Ru/MgO
Elektrokimya
Mikroemülsiyon

ÖZ

Elektrot malzemeleri, elektrokimyasal cihazların performansı ve ömrü açısından önemli bir bileşendir. Elektrokimyasal cihazlarda elektrot malzemesi olarak çeşitli metal ve metal oksit malzemeler kullanılmaktadır. Bu bağlamda bu malzemelerin elektrokimyasal özelliklerinin iyileştirilmesine yönelik çeşitli çalışmalar yapılmaktadır. Bu çalışmada enerji depolama cihazları için Ru/MgO metal/metal oksit nanomalzemesi sentezlenmiş ve elektrokimyasal özellikleri döngüsel voltametri (CV) ve galvanostatik şarj ve deşarj (GCD) yöntemleriyle incelenmiştir. MgO üzerinde homojen Ru nanopartikülleri elde edildi. XRD modeli kullanılarak yapılan hesaplamaya göre Ru nanopartiküllerinin kristal boyutu yaklaşık 4,2 nm idi. Farklı akım yoğunluklarında alınan GCD ölçümlerine göre en yüksek özgül kapasitans 0,5 A/g'de 239 F/g ile elde edilmiştir.

To Cite: Bozkurt G. Examination of the Electrochemical Behavior of Ru Nanoparticles Prepared on MgO. Osmaniye Korkut Ata Üniversitesi Fen Bilimleri Enstitüsü Dergisi 2024; 7(5): 2053-2064.

1. Introduction

The need for lightweight, low-cost, and high-performance power supplies is increasing day by day. Therefore, research on portable electronics is gaining importance (Ray and Saruhan 2020). Batteries and supercapacitors are long-life, lightweight, and low-cost energy storage devices that are very important for portable materials. In order to produce energy storage devices with the desired properties, the electrochemical properties of the electrode materials used in these devices need to be developed and improved. Various materials have been investigated in the literature as electrode materials for energy

storage devices. Among these, it is reported that transition metal oxides can provide various oxidation states for efficient redox charge transfer, resulting in much higher specific capacitance (Zhang et al. 2013). In general, monometallic transition metal oxides (such as NiO, CuO, Co_3O_4, Fe_3O_4, and Mn_3O_4), single-phase bimetallic oxides (such as $NiCo_2O_4$, $MnCo_2O_4$, $NiMoO_4$, $NiFe_2O_4$, and $CoMn_2O_4$) and noble metal oxides (such as RuO_2 and IrO_2) have been investigated as electrode materials (Wu et al. 2016). Additionally, transition metals are used in energy storage devices. However, it is known that not every metal is suitable. Precious metals such as Ag, Au, and Pt are not generally used due to their cost. Elements such as Hg and Cd are not safe materials for electrodes due to their toxicity. Ru is also a precious metal but has excellent electrochemical performance, especially in the oxide state, which is applied in the military industry (Xi 2022). Therefore, different metal or metal oxide materials can be used as electrode materials.

The type of support material used affects the size, distribution, and resistance to sintering of the deposited Ru particles (Javaid et al. 2020; Javaid et al. 2023). Ru/MgO has been investigated in various studies for ammonia decomposition and synthesis due to its high catalytic activity and stability (Ju et al. 2017; Ju et al. 2019; Wildfirea et al. 2021; Yamazaki et al. 2022; Fang et al. 2023; Javaid et al. 2023). However, no publication has been observed examining the galvanostatic charge-discharge based electrochemical properties of Ru/MgO.

In this work, MgO was synthesized by the microemulsion method. Then, Ru nanoparticles were supported on MgO by the solvothermal method and exposed to microwave treatment. The physical and electrochemical properties of the obtained Ru/MgO nanoparticles were examined to examine their use in energy storage devices.

2. Materials and Method

2.1. Materials

Magnesium chloride hexahydrate ($MgCl_2.6H_2O$, (≥99%)), Ruthenium (III) chloride ($RuCl_3$, 45-55%Ru content)), the surfactant dioctyl sulfosuccinate sodium salt (AOT, (≥97%)), n-heptane (99%), 1-butanol, and NaOH (≥98%), KOH (≥98%) and nafion (15-20% water) were obtained from Sigma–Aldrich. All aqueous solutions were prepared using distilled water.

2.2. Synthesis of MgO and Ru/MgO

MgO was achieved by using the microemulsion method. MgO was prepared as previously reported (Bozkurt and Daş 2023). Then, Ru nanoparticles were supported on MgO by the solvothermal method and exposed to microwave treatment as previously reported by Bozkurt (2023). Ru/MgO synthesis is given schematically in Figure 1. Ru metal loading on the MgO was set to 10 wt%.

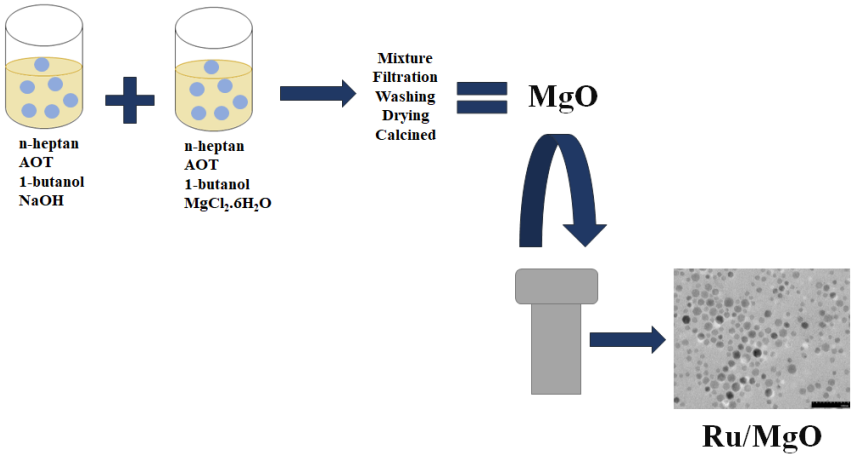

Figure 1. Schematic representation of the synthesis of Ru/MgO nanoparticles

2.3. Material Characterization

The structure of the nanocomposites was characterized by X-ray diffraction (XRD, PANalytical Empyrean). The morphology of the nanocomposites was investigated by a scanning electron microscope (SEM, Zeiss Sigma 300). The surface area, pore volume, and pore radius of the nanocomposites were measured using a BET instrument (Micromeritics 3Flex). The microstructure characterization of the nanocomposites was performed with a Hitachi HighTech HT7700 Transmission electron microscope (TEM). X-ray photoelectron spectroscopy analysis was carried out on the Specs-Flex X-ray photoelectron spectrometer. Inductively coupled plasma-mass spectrometer (ICP/MS) analysis was carried out on Agilent 7800 ICP-MS.

2.4. Electrochemical Characterization

CV and the GCD measurements of the Ru/MgO were investigated with a potentiostat/galvanostat (Gamry 1010E) connected to a three-electrode electrochemical cell system. The electrochemical experiments were performed using a conventional three-electrode cell. A glassy carbon disc electrode as a working electrode, platinum wire as a counter electrode, and an Ag/AgCl reference electrode were employed. An ink solution on a glassy carbon electrode was prepared with 20% nafion and distilled water by taking 50 µg of material/cm^2 from the Ru/MgO nanoparticles in powder form. The electrolyte solution is 1 M 100 ml of KOH solution. The experiments were carried out in the potential range of –0.5V/+0.5V and at different scanning rates of 10 to 200 mV/s. In addition, galvanostatic charge/discharge (GCD) measurements were performed. In addition, EIS experiments were carried out to determine the capacitive and resistive behavior of Ru/MgO. The frequency range for EIS measurements is 0.01 to 100000 Hz. The specific capacitance values were calculated according to the following equation:

$$C = \frac{1}{mv(V_C - V_a)} \int_{Va}^{Vc} Iv \, dV \qquad (1)$$

where C; specific capacitance (F/g), m; active mass of the electrode (g), ν; scan rate (mV/s), Iv; voltammetric current (A) and Vc-Va; sweep potential range is (V) (Deka et al. 2016).

3. Results and Discussion

3.1. Characterizations of the MgO and Ru/MgO

According to Figure 2, XRD analysis confirmed the typical structure of MgO. The peaks were consistent with MgO peaks (MATCH no. 96-901-6214). In addition, characteristic diffraction peaks at approximately 37.8 - 50.6 and 58.2° corresponding to (100), (101), and (102) planes of hexagonal close-packed (hcp) Ru were observed. The crystal size for Ru/MgO was calculated as 4.2 nm using the metallic Ru peak at approximately 50º with the help of the Scherrer equation.

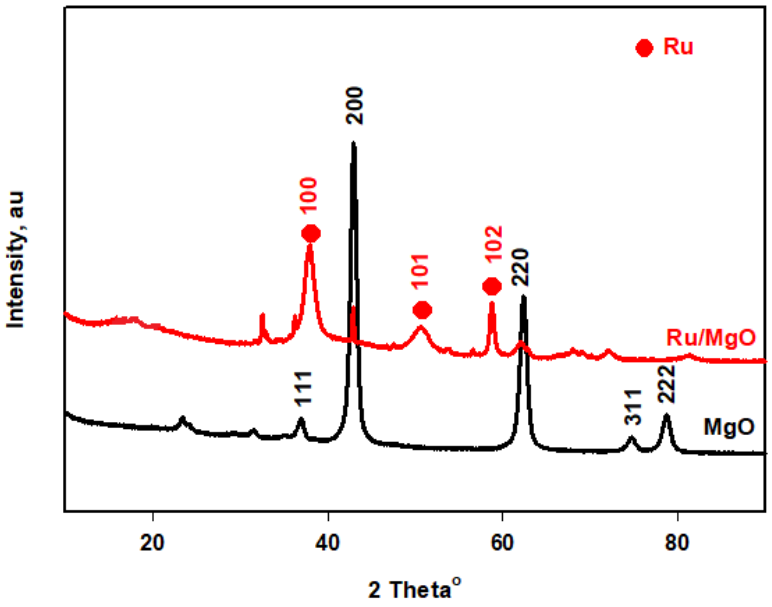

Figure 2. XRD patterns of MgO and Ru/MgO

Figure 3 illustrates the nitrogen adsorption-desorption isotherm (BET measurement curve) and BJH desorption pore volume graph for MgO. MgO showed a type IV isotherm associated with the mesoporous structure, and the surface area was 52.3 m^2/g. In addition, according to the pore distribution graph (inset graph), MgO showed a mesopore distribution observed between 2 and 50 nm.

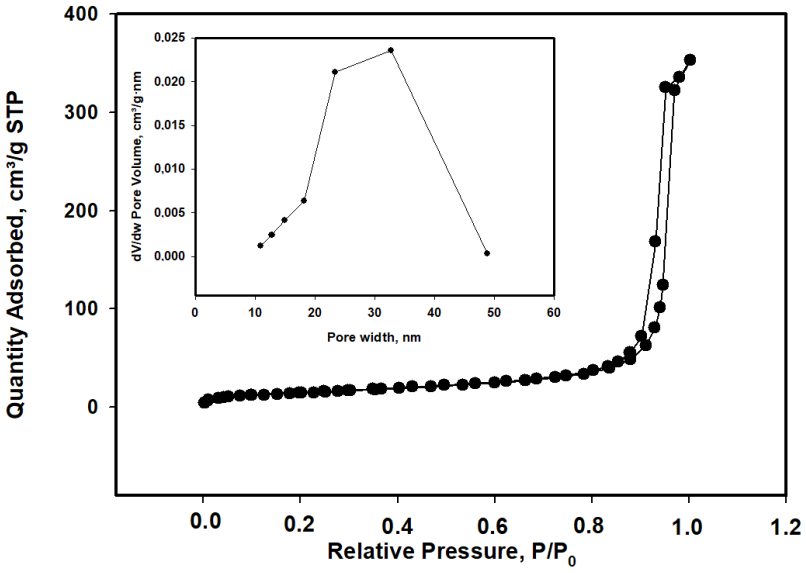

Figure 3. BET isotherms and BJH desorption pore volume distributions (inset graphs) of MgO

SEM images and EDS results for MgO and Ru/MgO are given in Figure 4. According to the SEM image in Figure 4a, nanoleaf structures were observed for MgO. According to the EDS result (Figure 4b), peaks of Mg and O were observed. According to the SEM image of Ru/MgO shown in Figure 4c, new structures were formed on top of the nanoleaf structures. Similarly, as a result of the EDS of Ru/MgO (Figure 4d), peaks for Ru, Mg, and O were observed.

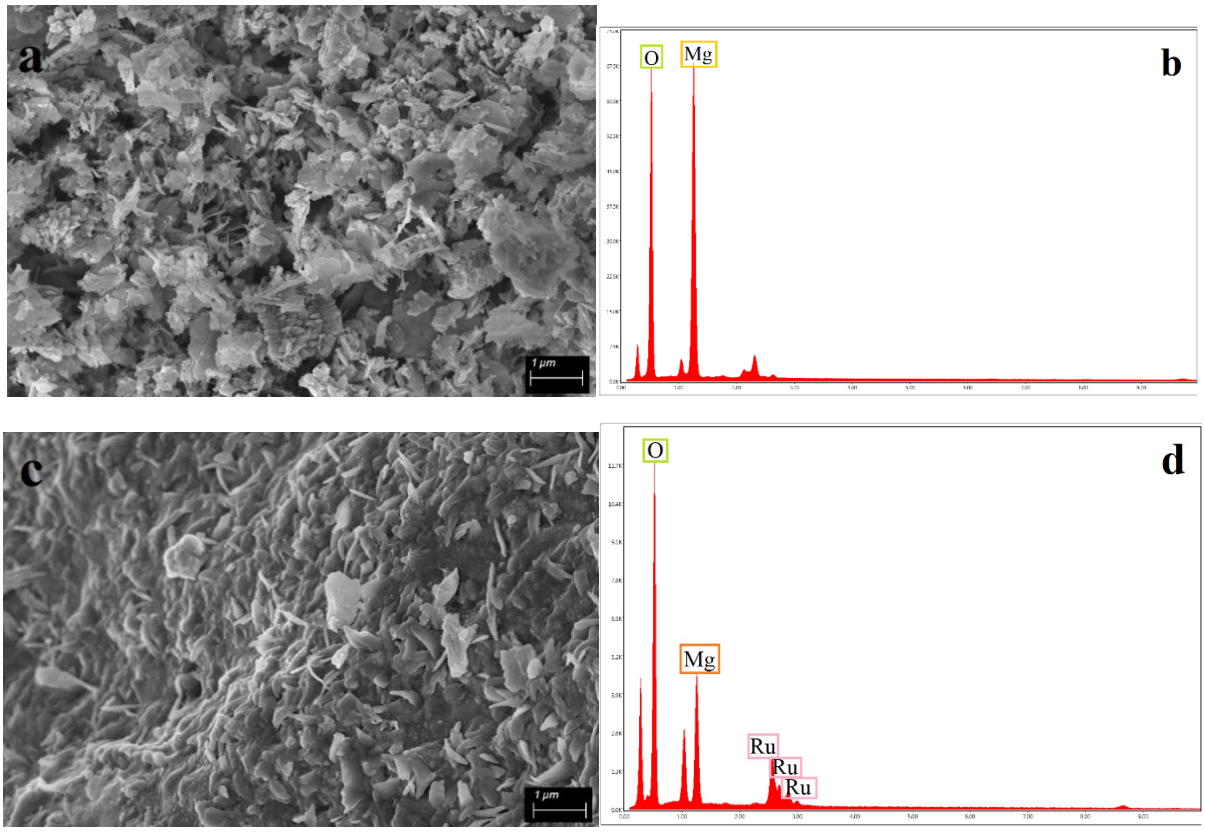

Figure 4. SEM images and EDS spectra of (a-b) MgO (c-d) Ru/MgO

TEM images of MgO are given in Figure 5a and Ru/MgO in 5b (500 nm scale) and 5c (100 nm scale). According to the TEM images, it was observed that Ru nanoparticles were distributed on MgO in spherical form. According to the histogram graph given in Figure 5d, the average particle size was calculated as 18.5 nm. Using the log-normal distribution function, a standard deviation of 1.18 nm was calculated.

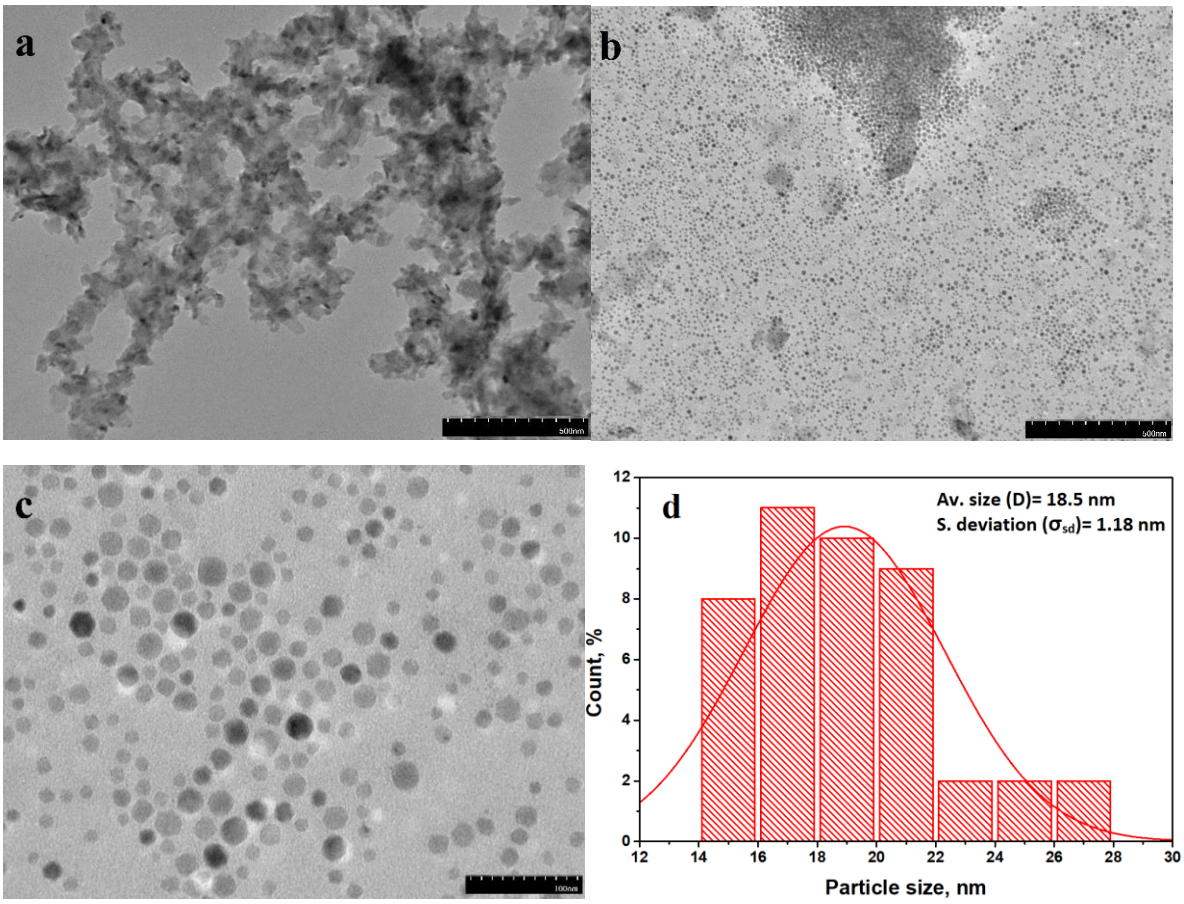

Figure 5. TEM images of (a) MgO (b) Ru/MgO (500 nm scale) (c) Ru/MgO (100 nm scale) (d) particle size distribution for Ru/MgO fitted with a log normal distribution function

The electronic properties of elements were obtained by XPS measurement, as shown in Figure 6. Figure 6a indicates the presence of Mg, O, and Ru. Accordingly, the Mg 1s spectrum exhibited one prominent peak resolved at 1306 eV, accompanied by a satellite (Figure 6b), which is directly related to the characteristic signals of MgO (Aboutalebianaraki et al. 2022). According to the O1s spectrum given in Figure 6c, the peaks at 532.3 eV and 531.7 eV are attributed to chemisorbed oxygen and crystal lattice oxygen, respectively (Leelavathi et al. 2013). According to Figure 6d–e, signals with binding energies consistent with Ru (0) were observed (Wu and Jiang 2015; Yinghuai 2007). According to Figure 6e, the metallic state of Ru, characterized by $Ru3p_{3/2}$ and $Ru3p_{1/2}$ peaks, was observed at 462.3 eV and 484.5 eV, respectively (Saptal et al. 2018). According to the ICP-MS analysis used to confirm the Ru content, the Ru loading percentage was found to be 8.6%.

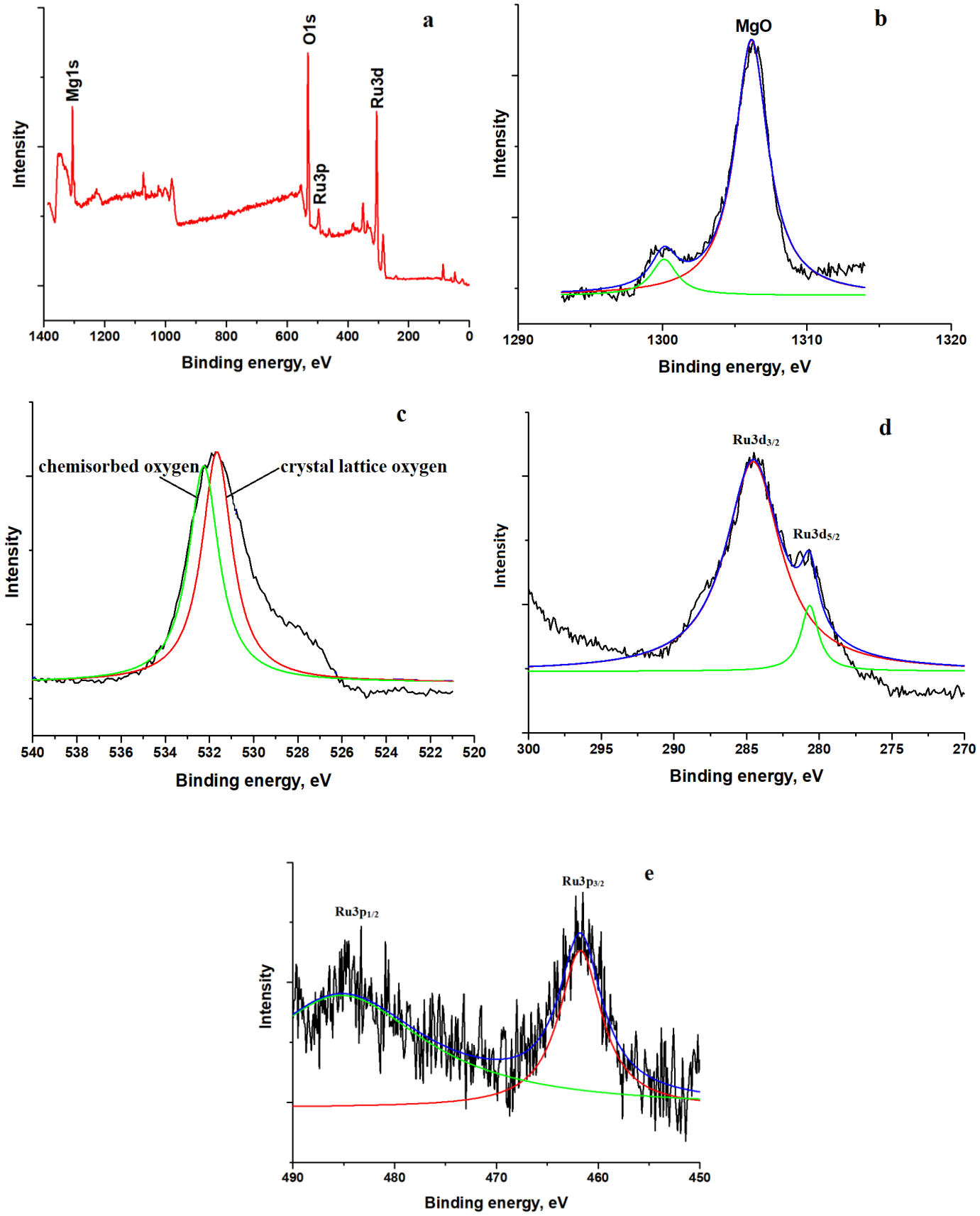

Figure 6. XPS spectrums for Ru-MgO (a) general spectrum (b) Mg 1s (c) O 1s (d) Ru 3d (e) Ru 3p regions

Figure 7 shows the results of electrochemical tests for Ru/MgO. As can be seen in Figure 7a, cyclic voltammetry measurements were performed over the potential range of -0.5 V to 0.5 V at five different scan rates including 10-20-50-100 and 200 mV/s. As the scanning speed increased, a rectangular-like cycle close to ideal capacitive behavior was obtained. As the scan rate increases, there is a high surface area with a high number of nanopores for maximum diffusion at the electrode/electrolyte interface. This results in an increase in capacitance (Ray et al. 2020). The specific capacitance increased in direct proportion to the increase in scan rate. In redox reactions that depend on the insertion or deinsertion of protons into the electrolyte at low scan rates, diffusion of ions from the electrolyte occurs in almost all available pores of the electrode. In this case, the insertion reaction occurs, and near-ideal capacitance behavior occurs. In addition, the effective interaction between ions and the electrode decreases significantly with increasing scan rates (Dubal et al 2013). In these (Figure 7a), taken at different scanning speeds, a slight anodic peak was observed at approximately -0.3 V. CV curves do not have a rectangular shape due to the faradaic pseudo-capacitive nature of the electrode, especially at high scanning speeds (Zhang et al. 2013). The galvanostatic charge-discharge cycle at various current densities was also investigated, as shown in Figure 7b. Specific capacitances were calculated from galvanostatic charge-discharge curves using the equation given in Equation 1. The calculated specific capacitance values were 239.0, 104.2, 27.5 and 21.4 F/g at 0.5, 1, 2, and 3 A/g. Table 1 summarizes the specific capacitance of previously reported various supercapacitor electrode materials. Carbon and cobalt-based materials are generally used as electrode materials for supercapacitors and batteries. According to Table 1, the Ru/MgO prepared in this study exhibited a promising specific capacitance among these materials.

Table 1. Comparison of specific capacitance for various materials in alkaline aqueous electrolytes reported in the literature

Material	Specific capacitance (F/g)	Current density (A/g)	Electrolyte	Reference
Nitrogen-doped graphene nanosheets	132.4	0.1	1 M KOH	Zheng et al. 2013
Macrochanneled activated carbon	196	1	6 M KOH	Li et al. 2014
Co/Cr_2O_3	248.1	1	1 M KOH	Bozkurt G. 2023
Defect introduced graphene sheets	256.0	1	1 M KOH	Qui et al. 2017
$MnCo_2O_{4.5}$	368	1	2 M KOH	Zhang et al. 2019
Co_3O_4-NiO/Graphene oxide	883.0	1	6 M KOH	Yang et al. 2020
Ru/MgO	239.0	0.5	1 M KOH	This work

In addition, Figure 7c shows the Nyquist graph obtained as a result of electrochemical impedance spectroscopy for Ru/MgO. Approximately semicircular regions at high frequency and linear regions at low frequency were obtained. The semicircle corresponds to the electrochemical response of Ru/MgO. It also provides information about the charge transfer kinetics of the material. The linear part is indicative

of diffusion processes, such as ion diffusion within the pores of the electrode material (Gaikwad et al. 2024). In addition, the Bode plot showing the phase shift between current signals and voltage is given in Figure 7d. A decrease in phase angles was observed with increasing frequency. As the frequency increases, the phase angle decreases, indicating that the material exhibits resistive behavior. Ru/MgO behaved capacitive at low frequencies and resistively at high frequencies (Gaikwad et al. 2024; Shafa et al. 2021).

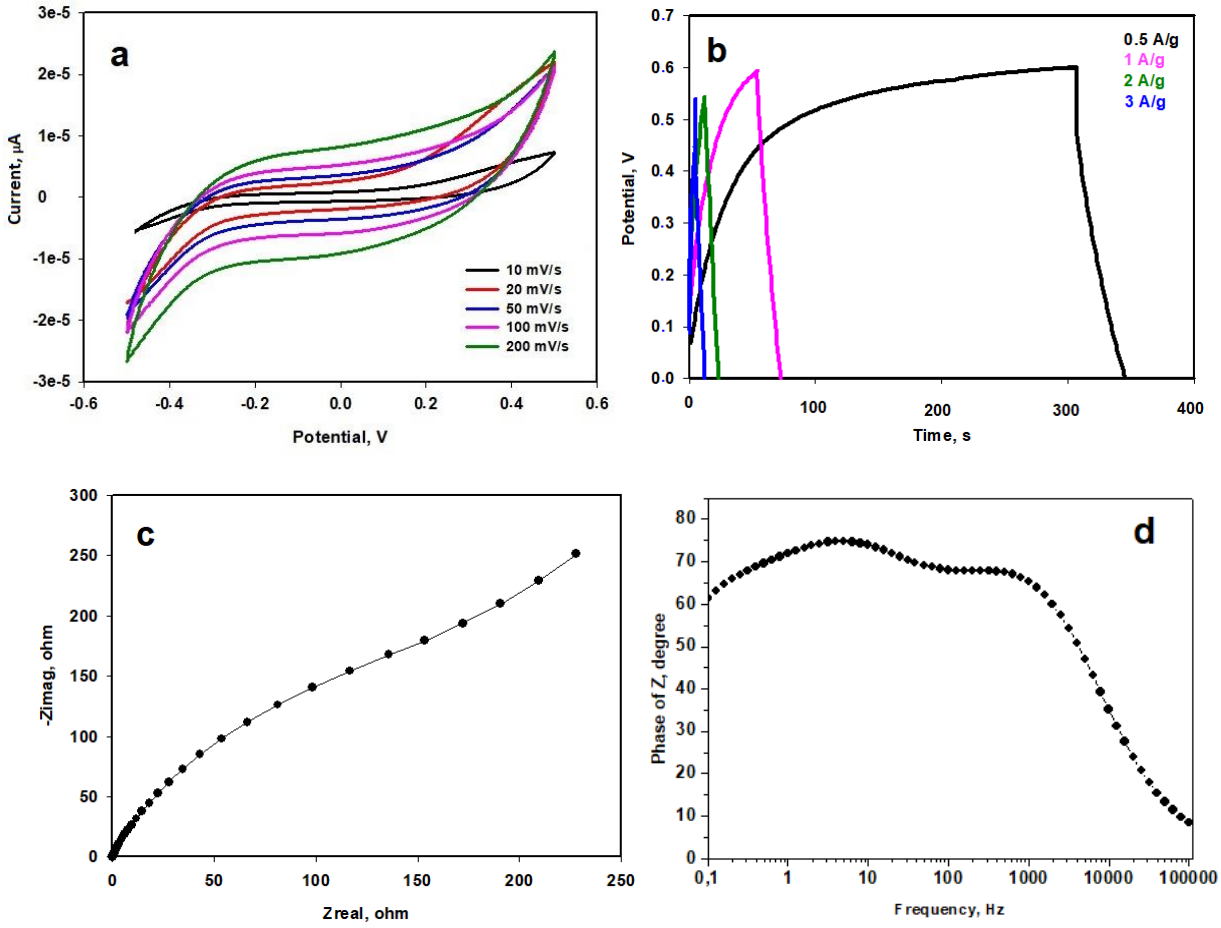

Figure 7. Electrochemical characteristics of the Ru-MgO (a) CV curves (b) GCD curves (c) EIS curves (d) Bode plots

4. Conclusions

In this study, Ru nanoparticles were prepared on MgO synthesized by the microemulsion method. According to the XRD pattern of the received Ru/MgO, the crystal size of Ru nanoparticles was calculated as 4.2 nm. In the TEM image of this material, which has a very small crystal size, nanoparticles with a homogeneous structure were clearly observed and the average particle size was found to be 18.5 nm. According to the XPS result, metallic Ru was obtained. According to the CV measurements were performed at different scan rates. It has been observed that as the scan rate increases, cycles closer to the rectangular-like cycle are formed. Additionally, GCD measurements were taken at various current densities. The highest specific capacitance of 239.0 F/g was achieved for 0.5 A/g. The

obtained specific capacitance value is promising for the use of Ru/MgO nanomaterials as electrode materials in energy storage devices.

Conflict of interest

The author declares no conflict of interest.

References

Aboutalebianaraki N., Neal CJ., Seal S., Razavi M. Biodegradable Mg-Sc-Sr Alloy improves osteogenesis and angiogenesis to accelerate bone defect restoration. Journal of Functional Biomaterials 2022; 13: 261-278.

Bozkurt YG. Investigation of electrochemical performance of Ni/Cr_2O_3 and Co/Cr_2O_3 composite nanoparticles prepared by microwave-assisted solvothermal method. Journal of Alloys and Compounds 2023; 960: 170627.

Bozkurt YG., Daş E. The synthesis of MgO and MgO-graphene nanocomposite materials and their diode and photodiode applications. Physica Scripta 2023; 98: 085911.

Deka BK., Hazarika A., Kim J., Park YB., Park HW. Multifunctional CuO nanowire embodied structural supercapacitor based on woven carbon fiber/ionic liquid–polyester resin. Composites: Part A, 2016; 87: 256-262.

Dubal DP., Gund GS., Holze R., Lokhande CD. Mild chemical strategy to grow micro-roses and micro-woolen like arranged CuO nanosheets for high performance supercapacitors. Journal of Power Sources 2013; 242: 687-698.

Fang H., Wu S., Ayvali T., Zheng J., Fellowes J. Dispersed surface Ru ensembles on MgO (111) for catalytic ammonia decomposition. Nature Communications 2023; 14: 647.

Gaikwad DS., Bobade RG., Suryawanshi VB., Nakate UT., Shaikh SF., Enizi A., Dabke DB., Lokhande BJ., Ambare RC. Electrochemical property of nanosphere-like MgO electrode synthesized via SILAR in asymmetric supercapacitor. Journal of Materials Science: Materials in Electronics 2024; 35: 363.

Javaid R., Aoki Y., Nanba T. Highly efficient Ru/MgO-Er_2O_3 catalysts for ammonia synthesis. Journal of Physics and Chemistry of Solids 2020; 146: 109570.

Javaid R., Nanba T. Efficient Ru/MgO–CeO_2 catalyst for ammonia synthesis as a hydrogen and energy carrier. International Journal of Hydrogen Energy 2023; 48(30): 11214-11224.

Ju X., Liu L., Yu P., Guo J., Zhang X. Mesoporous Ru/MgO prepared by a deposition-precipitation method as highly active catalyst for producing COx-free hydrogen from ammonia decomposition. Applied Catalysis B: Environmental 2017; 211: 167-175.

Ju X., Liu L., Zhang X., Feng J., He T., Chen P. Highly efficient Ru/MgO catalyst with surface-enriched basic sites for production of hydrogen from ammonia decomposition. Chem Cat Chem 2019; 11: 4161–4170.

Leelavathi A., Madras G., Ravishankar N. Origin of enhanced photocatalytic activity and photoconduction in high aspect ratio ZnO nanorod. Physical Chemistry Chemical Physics 2013; 15: 10795.

Li J., Ren Z., Ren Y., Zhao L., Wang S., Yu J. Activated carbon with micrometer-scale channels prepared from luffa sponge fibers and their application for supercapacitors. RSC Advances 2014; 4: 35789.

Qiu Z., He D., Wang Y., Zhao X., Zhao W., Wu H. High performance asymmetric supercapacitors with ultrahigh energy density based on hierarchical carbon nanotubes@NiO core–shell nanosheets and defect-introduced graphene sheets with hole structure. RSC Advances, 2017; 7: 7843.

Ray A., Korkut D., Saruhan B. Efficient flexible all-solid supercapacitors with direct sputter-grown needle-like Mn/MnOx@Graphite-Foil electrodes and PPC-embedded ionic electrolyte. Nanomaterials 2020; 10(9): 1768.

Saptal VB., Sasaki T., Bhanage BM. Ru@PsIL-Catalyzed Synthesis of N-formamides and benzimidazole by using carbon dioxide and dimethylamine borane. Chem Cat Chem 2018; 10: 1-9.

Shafai N., Beltagi A., Ibrahim MM., Ramadanc MS., Mehasseb I. Enhancement of the photocurrent and electrochemical properties of the modified nanohybrid composite membrane of cellulose/graphene oxide with magnesium oxide nanoparticle (GO@CMC.MgO) for photocatalytic antifouling and supercapacitors applications. Electrochimica Acta 2021; 392: 138989.

Wildfirea C., Abdelsayed V., Shekhawat D., Daglec RA., Davidson SD., Hu J. Microwave-assisted ammonia synthesis over Ru/MgO catalysts at ambient pressure. Catalysis Today 2021; 365: 103-110.

Wu Z., Jiang H. Efficient palladium and ruthenium nanocatalysts stabilized by phosphine functionalized ionic liquid for selective hydrogenation. RSC Advances 2015; 5: 34622.

Wu Z., Zhu Y., Ji X., Banks CE. Nanomaterials in advanced batteries and supercapacitors. In: Ozoemena, K.I., Chen, S (editors). Transition metal oxides as supercapacitor materials. Nanomaterials in Advanced Batteries and Supercapacitors. Part 9. Canada: Springer, 2016; 317-344.

Xi Z. Recent advances of transition metal oxides and chalcogenides in pseudo-capacitors and hybrid capacitors: A review of structures, synthetic strategies, and mechanism studies. Journal of Energy Storage 2022; 49: 104148.

Yamazaki K., Matsumoto M., Kubo H., Fujitani T., Ishikawa M., Sato A. Evaluation of durability performance of a Ru/MgO catalyst for ammonia decomposition at an on-site hydrogen fueling station. Industrial & Engineering Chemistry Research 2022; 61(17): 5778–5785.

Yang X., Xiang C., Zou Y., Liang J., Zhang H., Yan E., Xu F., Hu X., Cheng Q., Sun L. Low-temperature synthesis of sea urchin-like Co-Ni oxide on graphene oxide for supercapacitor electrodes. Journal of Materials Science & Technology 2020: 55: 223-230.

Yinghuai Z., Widjaja E., Sia SL., Zhan W. Carpenter K et al. Ruthenium (0) nanoparticle-catalyzed isotope exchange between 10B and 11B nuclei in decaborane (14). Journal of the American Chemical Society 2007; 129(20): 6507–6512.

Zhang YX., Li F., Huang M. One-step hydrothermal synthesis of hierarchical MnO_2-coated CuO flower-like nanostructures with enhanced electrochemical properties for supercapacitor.Materials Letters 2013; 112: 203-206.

Zhang M., Liu W., Liang R., Tjandra R., Yu A. Graphene quantum dot induced tunable growth of nanostructured $MnCo_2O_{4.5}$ composites for high-performance supercapacitors Sustainable Energy Fuels 2019: 3: 2499-2508.

Zheng B., Chen T., Xiao FN., Bao WJ., Xia XH. KOH-activated nitrogen-doped graphene by means of thermal annealing for supercapacitor. Journal of Solid-State Electrochemistry 2013; 17: 1809–1814.